

Zwitterionic dithiocarboxylates derived from *N*-heterocyclic carbenes: coordination to gold surfaces†Ulrich Siemeling,<sup>\*a,c</sup> Henry Memczak,<sup>‡a,c</sup> Clemens Bruhn,<sup>a</sup> Florian Vogel,<sup>b,c</sup> Frank Träger,<sup>b,c</sup> Joe E. Baio<sup>d</sup> and Tobias Weidner<sup>d</sup>

Received 19th October 2011, Accepted 5th December 2011

DOI: 10.1039/c2dt11976e

The zwitterionic dithiocarboxylates  $1^+-CS_2^-$ – $4^+-CS_2^-$  were prepared by reacting the corresponding *N*-heterocyclic carbenes 1,3-bis(2,6-diisopropylphenyl)imidazol-2-ylidene (**1**), 1,3-diisopropylimidazol-2-ylidene (**2**), 1,3-dibenzylimidazol-2-ylidene (**3**) and 1,3-diethylbenzimidazol-2-ylidene (**4**) with  $CS_2$ . In the latter two cases, the corresponding *N*-heterocyclic carbene was generated *in situ*. Compounds  $2^+-CS_2^-$ – $4^+-CS_2^-$  were structurally characterised by single-crystal X-ray diffraction studies. The chemisorption of these zwitterionic dithiocarboxylates on solid gold substrates was investigated *in situ* and in real time by optical second harmonic generation (SHG). The resulting thin films were exemplarily characterised by near-edge X-ray absorption fine structure (NEXAFS) spectroscopy and X-ray photoelectron spectroscopy (XPS) in the case of  $1^+-CS_2^-$  and  $2^+-CS_2^-$ , revealing the formation of almost contamination-free self-assembled monolayers, which exhibit a remarkable degree of orientational order.

## Introduction

Owing to their high nucleophilicity, *N*-heterocyclic carbenes (NHCs) react with carbon disulfide, affording zwitterionic dithiocarboxylates of the general type  $NHC^+-CS_2^-$ .<sup>1</sup> First examples of such compounds had been prepared less straightforwardly from enetetramines and  $CS_2$  already several decades ago.<sup>2</sup> These pseudo-cross-conjugated mesomeric betaines<sup>3</sup> are currently attracting great interest. Their potential for probing the stereoelectronic parameters of NHCs was recently investigated by Delaude *et al.*<sup>4</sup> They have been utilised as efficient organocatalysts,<sup>5</sup> and their application as ligands, which is based on sporadic work in the 1980s,<sup>6</sup> is a highly dynamic area of transition-metal coordination chemistry.<sup>7</sup> Very recently, Delaude, Wilton-Ely and co-workers have demonstrated that zwitterionic dithiocarboxylates  $NHC^+-CS_2^-$  are also suitable for the stabilisation of gold nanoparticles.<sup>7c</sup> This has prompted us to study their chemisorption on solid gold substrates. The present investigation

is part of our programme addressing the multipoint attachment of bi-<sup>8</sup> and oligodentate<sup>9</sup> adsorbate species on gold. We note that Lee and coworkers have shown that dithiocarboxylic acids  $R-CS_2H$  ( $R = n$ -alkyl) form self-assembled monolayers (SAMs) on gold.<sup>10</sup> Such SAMs contain surface-bound anionic dithiocarboxylate groups  $R-CS_2^-$ , while SAMs fabricated from zwitterionic dithiocarboxylates  $NHC^+-CS_2^-$  are expected to contain intact, neutral adsorbate molecules. In general, zwitterionic ligands are an attractive alternative to anionic ligands like thiolates, because they can become attached to metallic substrates without a change of the oxidation state of the surface metal atoms.

## Results and discussion

## Synthetic work and crystal structures

The nucleophilic addition reactions of the NHCs **1–4** with an excess of  $CS_2$  in THF afforded the corresponding zwitterionic dithiocarboxylates  $1^+-CS_2^-$ – $4^+-CS_2^-$  as red solids in good yield (Scheme 1). While the 2,6-diisopropylphenyl-substituted imidazol-2-ylidene **1** and the isopropyl-substituted imidazol-2-ylidene **2** were synthesised and isolated as crystalline solids by well-established methods,<sup>11</sup> the benzyl-substituted imidazol-2-ylidene **3** and the ethyl-substituted benzimidazol-2-ylidene **4** were generated for this purpose *in situ* by deprotonation of  $[3H]Cl$ <sup>12</sup> and  $[4H]Br$ ,<sup>13</sup> respectively.  $1^+-CS_2^-$  had already been obtained previously by Delaude *et al.* in lower yields by the *in situ* method and was characterised crystallographically by these authors.<sup>4</sup> Although  $2^+-CS_2^-$  was used as a ligand in a recent study, preparative and analytical details have been unavailable for this compound.<sup>7a,c</sup>

<sup>a</sup>Institute of Chemistry, University of Kassel, Heinrich-Plett-Str. 40, 34132 Kassel, Germany. E-mail: siemeling@uni-kassel.de

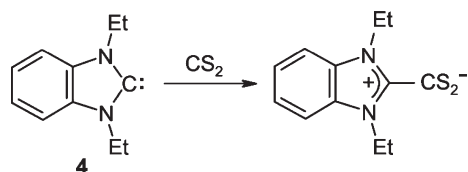
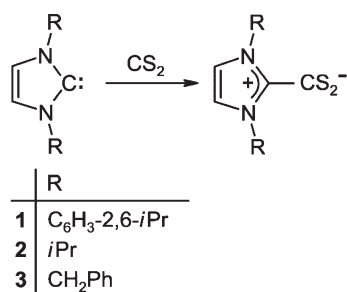
<sup>b</sup>Institute of Physics, University of Kassel, Heinrich-Plett-Str. 40, 34132 Kassel, Germany

<sup>c</sup>Center for Interdisciplinary Nanostructure Science and Technology, University of Kassel, Heinrich-Plett-Str. 40, 34132 Kassel, Germany

<sup>d</sup>National ESCA and Surface Analysis Center for Biomedical Problems (NESAC/BIO), Departments of Bioengineering and Chemical Engineering, University of Washington, Seattle, Washington 98195, USA

† Electronic supplementary information (ESI) available: Fig. S1 showing the pleochroitic behaviour of compound  $3^+-CS_2^-$ . CCDC reference numbers 847616–847618. For ESI and crystallographic data in CIF or other electronic format see DOI: 10.1039/c2dt11976e

‡ Current address: Fraunhofer Institute for Biomedical Engineering, Am Mühlenberg 13, 14476 Potsdam-Golm, Germany.



**Scheme 1** Synthesis of the zwitterionic dithiocarboxylates for  $1^+-CS_2^-$ – $4^+-CS_2^-$ .

We have carried out single-crystal X-ray diffraction studies for  $2^+-CS_2^-$ – $4^+-CS_2^-$ . The molecular structures of these compounds are shown in Fig. 1–3. Pertinent bond parameters are collected in Table 1, which also includes the corresponding data of  $1^+-CS_2^-$  for comparison. As a sideline of our crystallographic investigation we note that single-crystals of the benzyl-substituted compound  $3^+-CS_2^-$  exhibit strong pleochroism (see ESI, Fig. S1†). Bond lengths and angles compare well to those of other compounds of the type  $NHC^+-CS_2^-$ .<sup>1a,4</sup> The only remarkable feature occurs in the case of the benzyl-substituted  $3^+-$

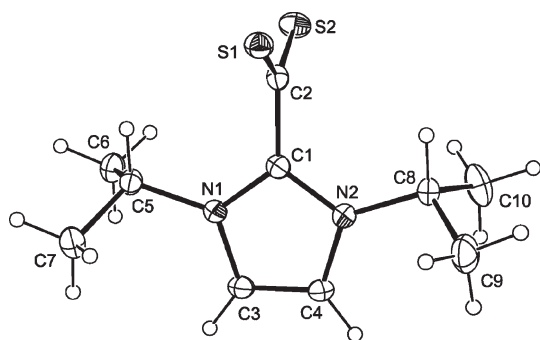


**Fig. 1** Molecular structure of  $2^+-CS_2^-$  in the crystal. Thermal ellipsoids are drawn at the 30% probability level.

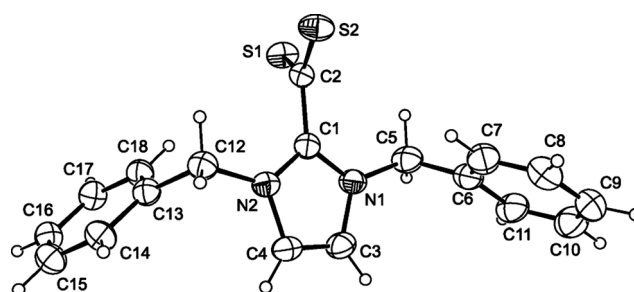


**Fig. 2** Molecular structure of  $3^+-CS_2^-$  in the crystal. Only one of the two independent molecules is shown. Thermal ellipsoids are drawn at the 30% probability level.

$CS_2^-$ , which does not show the approximately orthogonal orientation of the  $CS_2$  and  $CN_2$  planes which is usually found for such zwitterionic compounds. The two independent molecules of  $3^+-CS_2^-$  exhibit a deviation from orthogonality of *ca.* 20° and *ca.* 30°, respectively, as is indicated by their N–C–S torsion angle values (molecule 1: 71.55°, –109.25°, –107.39°, 71.81°; molecule 2: –60.10°, 121.22°, 118.62°, –60.06°).

All compounds were further characterised by pertinent spectroscopic methods. Their characteristic red colour originates from  $CS_2^-$ -based  $n \rightarrow \pi^*$  transitions.<sup>6b,14</sup> Optical spectroscopy revealed that the corresponding absorption maximum is located at *ca.* 530 nm in all cases (dichloromethane solution). Compounds  $2^+-$

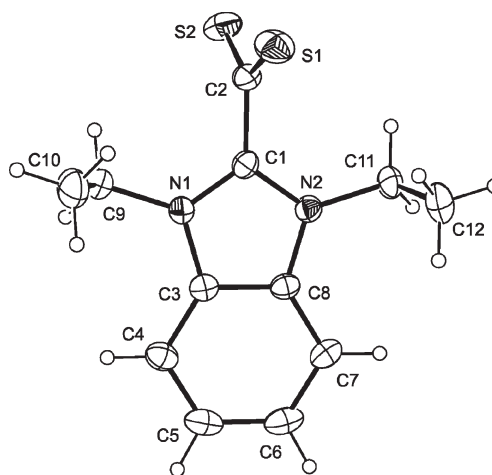


**Fig. 3** Molecular structure of  $4^+-CS_2^-$  in the crystal. Thermal ellipsoids are drawn at the 30% probability level.

**Table 1** Selected bond lengths (Å) and angles (°) for compounds  $1^+-CS_2^-$ – $4^+-CS_2^-$

Compound	C–CS <sub>2</sub>	C–S	N–CCS <sub>2</sub>	N–C–N	S–C–S	
$1^+-CS_2^-$	1.487(2)	1.659(5)	1.341(2)	107.5(1)	128.5(2)	Ref. 4
$2^+-CS_2^-$	1.485(4)	1.676(3)	1.387(1)	107.0(2)	130.5(2)	This work
$3^+-CS_2^-$	1.507(6)	1.675(3)	1.351(3)	108.0(4)	129.8(3)	This work
2 molecules	1.500(6)	1.677(3)	1.356(3)	107.0(4)	129.0(3)	
		1.674(5)	1.337(6)			
		1.675(5)	1.346(6)			
		1.674(5)	1.348(6)			
		1.677(5)	1.365(6)			
$4^+-CS_2^-$	1.499(6)	1.668(5)	1.340(5)	109.5(4)	130.6(3)	This work
		1.669(5)	1.342(5)			

$\text{CS}_2^-$ - $4^+$ - $\text{CS}_2^-$ , which carry aliphatic *N*-substituents, exhibit a second  $n \rightarrow \pi^*$  absorption at slightly higher energy ( $\lambda_{\text{max}}$  ca. 440 nm). In addition to these fairly weak bands ( $\log \epsilon$  ca. 2) in the visible region the  $\text{CS}_2^-$  group gives rise to an intense  $\pi \rightarrow \pi^*$  absorption in the UV region ( $\lambda_{\text{max}}$  ca. 360 nm,  $\log \epsilon$  ca. 4). The ring systems are responsible for  $\pi \rightarrow \pi^*$  bands of similar intensity ( $\log \epsilon$  ca. 4) at higher energy. While two absorption maxima located at ca. 235 and 260 nm are observed for the imidazolium-based compounds  $1^+$ - $\text{CS}_2^-$ - $3^+$ - $\text{CS}_2^-$ , the benzimidazolium-based derivative  $4^+$ - $\text{CS}_2^-$  exhibits three  $\pi \rightarrow \pi^*$  absorptions ( $\lambda_{\text{max}} = 229, 273, 309$  nm).

The charge delocalisation in the  $\text{CS}_2^-$  and  $\text{CN}_2^+$  parts of the zwitterions, as indicated already by the essentially identical carbon-heteroatom bond lengths in each unit (Table 1), is nicely reflected by characteristic data from vibrational spectroscopy. The highest intensity band in the Raman spectra is located in the narrow range between ca. 1465 and 1490  $\text{cm}^{-1}$  for these compounds and can be attributed to the  $\nu_s(\text{CN}_2^+)$  vibrational mode. The corresponding  $\nu_{\text{as}}(\text{CN}_2^+)$  vibrational band was observed between ca. 1465 and 1500  $\text{cm}^{-1}$  in the IR spectra, which further exhibit the characteristic  $\nu_{\text{as}}(\text{CS}_2^-)$  vibrational band between ca. 1045 and 1060  $\text{cm}^{-1}$ , in line with previously reported experimental findings for  $1^+$ - $\text{CS}_2^-$  and analogous compounds<sup>4</sup> and results of *ab initio* calculations.<sup>15</sup>

The  $\text{CN}_2^+$  and  $\text{CS}_2^-$  units give rise to  $^{13}\text{C}$  NMR signals at ca. 150 ppm and 220–225 ppm, respectively, which agrees very well with data reported for closely related compounds.<sup>1d,4</sup>

### SAM fabrication and investigation of the chemisorption process by optical second harmonic generation (SHG)

SAMs of  $1^+$ - $\text{CS}_2^-$ - $4^+$ - $\text{CS}_2^-$  were prepared from solution on solid gold substrates by applying a standard protocol (dichloromethane, room temperature, immersion time ca. 20 h). The SAM formation process was investigated *in situ* and in real time by optical second harmonic generation (SHG).<sup>16</sup> The SHG signal of the clean substrate in pure dichloromethane was recorded for reference purposes. Subsequently, the pure solvent was replaced by a dichloromethane solution of the adsorbate species, and the SHG signal was instantly monitored *in situ* as a function of time. The results of this SHG study are described here exemplarily for  $1^+$ - $\text{CS}_2^-$ . The other compounds showed similar behaviour. Fig. 4 shows the real-time SHG signal of the adsorption of this compound on the gold substrate for two different concentrations, *viz.*  $c = 50 \mu\text{mol L}^{-1}$  and  $c = 100 \mu\text{mol L}^{-1}$ . At  $t < 0$  the signal of the plain gold substrate immersed in pure solvent is measured. This signal has been set to unity. The change of the pure solvent to the solution of the adsorbate species causes an abrupt decrease of the SHG signal at  $t = 0$  and subsequently a decrease of the SHG signal is observed until saturation is reached.

The SHG data indicate similar adsorption behaviour for both concentrations. Not surprisingly, the adsorption process takes slightly longer for  $c = 50 \mu\text{mol L}^{-1}$  than for  $c = 100 \mu\text{mol L}^{-1}$ , as is indicated by the time needed to reach saturation of the SHG signal in each case, *viz.*  $t = (3500 \pm 500)$  s for  $c = 100 \mu\text{mol L}^{-1}$  and  $t = (4500 \pm 500)$  s for  $c = 50 \mu\text{mol L}^{-1}$ . In both cases a drop-off of the intensity of the SHG signal to  $0.80 \pm 0.02$  is observed. A decrease of the SHG signal was also noticed before

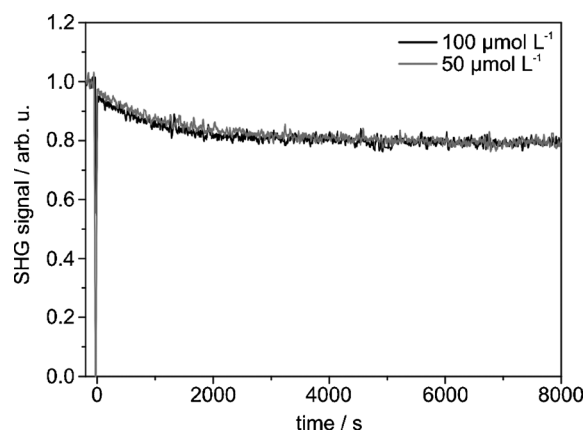


**Fig. 4** SHG signal recorded *in situ* and in real time during the adsorption of  $1^+$ - $\text{CS}_2^-$  onto a gold substrate from a  $100 \mu\text{mol L}^{-1}$  (black curve) and a  $50 \mu\text{mol L}^{-1}$  dichloromethane solution (grey curve), respectively.

for a wide variety of sulfur-based adsorbate species such as, for example, thiols,<sup>17</sup> thioethers,<sup>9d,18</sup> disulfides<sup>18</sup> and dithiolane derivatives.<sup>8b</sup> This behaviour can be explained by a decrease of the number of free electrons at the surface of the gold substrate by localisation in chemical bonds between the gold atoms and the adsorbing molecules. SHG is not suitable for probing the nature of these bonds on the surface. This can be achieved, however, by XPS and NEXAFS spectroscopy (*vide infra*).

From the SHG data, we can calculate the coverage  $\Theta$  of adsorbate molecules on the gold surface. If the SHG signal is saturated, the surface coverage is defined as  $\Theta = 1$ . The temporal development of the surface coverage  $\Theta$  is shown in Fig. 5a for  $c = 100 \mu\text{mol L}^{-1}$  and in Fig. 5d for  $c = 50 \mu\text{mol L}^{-1}$ . The adsorption kinetics can now be compared to three kinetic models which have been proposed in earlier studies to describe the formation of SAMs: (i) the first-order Langmuir model (FO), *i. e.* direct chemisorption of the molecules from the solution;<sup>19</sup> (ii) the second-order non-diffusion limited model (SO) involving the combined chemisorption of two groups present in one molecule;<sup>20</sup> (iii) the diffusion-limited Langmuir model (DL), *i. e.* diffusion of the molecules from the solution to the surface must be taken into account.<sup>19a</sup> Fig. 5b–c displays the agreement of the kinetic models with the surface coverage data for  $c = 100 \mu\text{mol L}^{-1}$ . For  $c = 50 \mu\text{mol L}^{-1}$ , this is shown in Fig. 5e–f. The abscissae are chosen in such a way that the experimental coverage data should follow a straight line for the respective kinetic model. For  $c = 100 \mu\text{mol L}^{-1}$ , all kinetic models show small deviations from the experimental data (*cf.* Fig. 5b–c). The best fit occurs with the SO model, which is expected to be particularly suitable for the theoretical description of the adsorption of  $1^+$ - $\text{CS}_2^-$  on gold surfaces, since two binding events can occur with the bidentate dithiocarboxylate headgroup. Obviously, for a concentration of  $c = 50 \mu\text{mol L}^{-1}$  the DL model fails to describe the experimental data. The FO model shows much smaller deviations from the data, but again the SO model is most consistent with the measurements. The rate-limiting step for the adsorption of  $1^+$ - $\text{CS}_2^-$  on gold surfaces therefore appears to be the formation of two gold–sulfur bonds between the headgroup and the surface atoms.

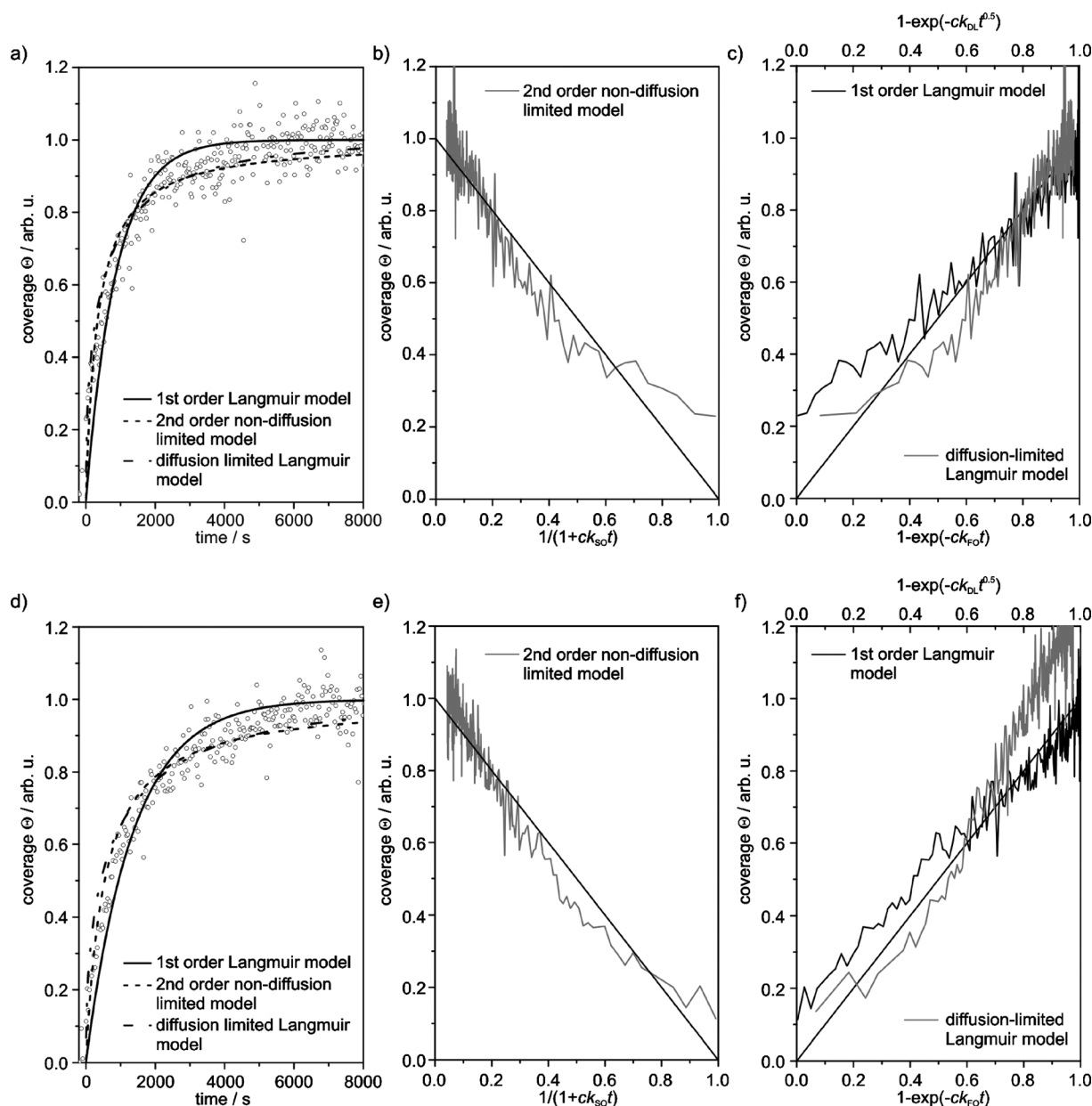


**Fig. 5** Coverage of  $1^+-CS_2^-$  on the gold substrate as a function of time for a concentration of  $100 \mu\text{mol L}^{-1}$  (a) and  $50 \mu\text{mol L}^{-1}$  (d). Coverage as a function of the kinetic model for  $100 \mu\text{mol L}^{-1}$  (b and c) and  $50 \mu\text{mol L}^{-1}$  (e and f); the abscissae are chosen such that for the corresponding model the coverage data should follow a straight line.

### SAM characterisation

**XPS results.** Surface characterisation was exemplarily performed for SAMs fabricated from compounds  $1^+-CS_2^-$  and  $2^+-CS_2^-$ , respectively. Elemental compositions of these SAMs were determined by X-ray photoelectron spectroscopy (XPS), which showed the presence of carbon, nitrogen, sulfur, oxygen, and gold (from the underlying substrate). The oxygen observed at the surface can be attributed to minimal substrate contamination prior to the film assembly, since no significant oxidation was indicated by the high-resolution XP spectra or the near-edge X-ray absorption fine structure (NEXAFS) data discussed later. Once the gold contribution is omitted (Table 2) the experimental

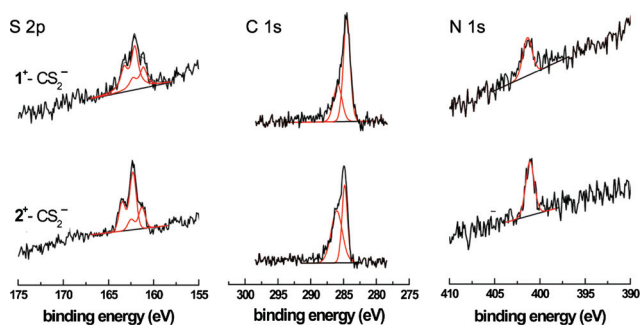
compositions fall into agreement with the stoichiometry of the two adsorbates. The only significant differences between theoretical and experimental compositions are that the atomic percentages of S and N are lower than expected (3.8 versus 14.3 sulfur at% in the case of  $2^+-CS_2^-$ ). If well-ordered monolayers are formed the sulfur and nitrogen containing groups are close to the gold surface and covered by the rest of the molecule. Thus, these lower percentages can be explained by attenuation of the sulfur and nitrogen signals due to inelastic scattering.

Fig. 6 shows high-resolution S 2p, C 1 s and N 1 s XP spectra for both SAMs on Au. The C 1 s spectra consist of two features, one at 284.9 eV corresponding to the alkyl chains and aromatic carbon rings and a high-energy shoulder at 286.0 eV that can be

**Table 2** Summary of XPS determined elemental compositions<sup>a</sup> for thin films of  $1^+-CS_2^-$  and  $2^+-CS_2^-$  on gold

		Au	C	N	S	O
$1^+-CS_2^-$	Theor. comp.	0	87.5	6.25	6.25	0
	Exp. comp.	65.4(2.8)	19.9(1.9)	1.9(0.6)	2.2(0.3)	2.2(0.9)
	Exp. comp. w/o Au	0	81.7(2.1)	5.5(1.5)	6.4(1.3)	6.4(2.1)
$2^+-CS_2^-$	Theor. comp.	0	71.4	14.3	14.3	0
	Exp. comp.	59.9(2.3)	33.1(0.9)	3.2(0.8)	3.8(0.3)	n. d. <sup>b</sup>
	Exp. comp. w/o Au	0	82.5(2.2)	8.0(2.0)	9.5(0.7)	n. d. <sup>b</sup>

<sup>a</sup> Values in at% with experimental errors in parentheses. <sup>b</sup> Not detected.



**Fig. 6** High-resolution S 2p (left), C 1s (middle) and N 1s (right) XPS spectra of SAMs fabricated from  $1^+-CS_2^-$  (top) and  $2^+-CS_2^-$  (bottom) on gold.

assigned to the C–N and C–S groups.<sup>21</sup> The broader width of the shoulder, as compared to the C–C emission, may also reflect contributions from small amounts of C–O contaminations of the substrate. This shoulder is double in size to what was expected just from stoichiometry for the SAM fabricated from  $2^+-CS_2^-$  (Table 3). Both SAMs contain only small amounts of oxygen, *viz.* 2–7 at%, which is similar to the oxygen content of the adventitious carbon layer we typically observe on our gold substrates (*ca.* 5 at%) prior to adsorption.

The N 1s spectra of both SAMs exhibit a single feature at 401.1 eV related to the N–C bonds.<sup>21</sup> The S 2p spectra exhibit two S 2p<sub>3/2,1/2</sub> doublets with binding energies (BE) of 162.2 and 161.2 eV and show no indication of oxidised sulfur species. The ratio between the area of the peak at 162.2 eV and that of the peak at 161.2 eV is 2 : 1 and 3 : 1, respectively, for the SAMs fabricated from  $1^+-CS_2^-$  and  $2^+-CS_2^-$  (Table 3). These two different doublets stem from two different sulfur species. The peak at 162.2 eV can be clearly assigned a gold-bound thiolate group.<sup>22</sup> The emission near 161.2 eV has been assigned to thiolate in a different binding geometry<sup>23</sup> or, in the case of the

closely related dithiocarbamates, to a monodentate surface binding with one sulfur atom bound to a counter ion.<sup>24</sup> Since no such counter ions have been detected with XPS, the BE difference between these two doublets is most likely the result of different hybridisation states or binding geometries of a bidentate binding configuration.<sup>9d</sup> This hypothesis is supported by results from the molecular coordination chemistry of dithiocarboxylates.<sup>25</sup> Several binding modes have been observed for structurally characterised Au<sup>I</sup> compounds, *viz.* monodentate,<sup>26</sup> chelating bidentate<sup>26a</sup> and bridging bidentate.<sup>27</sup> However, homoleptic complexes exclusively exhibit bridging bidentate dithiocarboxylate ligands, which strongly supports the notion that this is the preferred binding configuration in the case of dithiocarboxylate-based SAMs on gold, as has already been proposed by Lee and coworkers.<sup>10c,d</sup>

The effective film thickness of the SAMs was determined from the intensities of the C 1s and the Au 4f emissions. The thickness values were derived from the  $I_{C1s}/I_{Au4f}$  intensity ratios. We calculated thickness values of 10.0 and 9.5 Å, respectively, for the SAMs fabricated from  $1^+-CS_2^-$  and  $2^+-CS_2^-$  by using previously reported attenuation lengths,<sup>28</sup> this is in excellent agreement with monolayers on gold, since the expected thickness derived from the crystal structures (*vide supra*) is *ca.* 10 Å.

**NEXAFS spectroscopy.** The molecular orientation and alignment in SAMs prepared from  $1^+-CS_2^-$  and  $2^+-CS_2^-$  on gold surfaces were studied with NEXAFS spectroscopy. This method is extremely surface-sensitive and can provide information about the nature and orientation of chemical bonds of adsorbate species. Molecular orbitals are probed by monitoring resonant transitions of atomic core electrons into unoccupied molecular orbitals. The efficiency of the photoexcitation process is strongly dependent on the orientation of the X-ray electric field vector with respect to the molecular transition dipole moment (TDM). This effect is known as the linear dichroism of X-ray absorption and can be conveniently monitored by recording NEXAFS spectra with p-polarised X-rays at different incidence angles.<sup>29</sup>

**Table 3** High-resolution XPS C 1s peak fit results<sup>a</sup> for thin films of  $1^+-CS_2^-$  and  $2^+-CS_2^-$  on gold

		C–H <sub>n</sub> , C=C (284.9 eV)	C–N, C–S (286.0 eV)	Thiolate S (162.2 eV)	“Different” Thiolate S (161.2 eV)
$1^+-CS_2^-$	Theor. comp.	87.5	12.5		
	Exp. comp.	73.5	26.6	64.8	35.2
$2^+-CS_2^-$	Theor. comp.	71.4	28.6		
	Exp. comp.	42.4	57.6	73.0	27.0

<sup>a</sup> Values in at%.

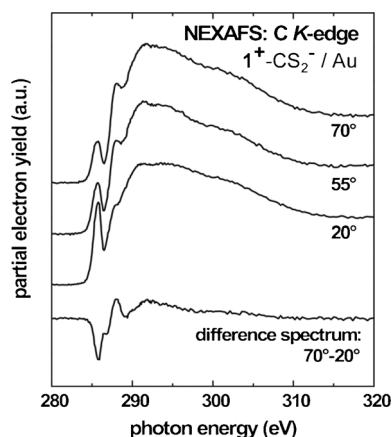


**Fig. 7** C K-edge NEXAFS spectra of SAMs prepared from  $1^+-CS_2^-$  acquired at X-ray incidence angles of  $70^\circ$ ,  $55^\circ$ , and  $20^\circ$ . The bottom curve represents the difference between the  $70^\circ$  and  $20^\circ$  spectra.

Fig. 7 and 8 show C K-edge NEXAFS spectra recorded at X-ray incidence angles of  $70^\circ$ ,  $55^\circ$  and  $20^\circ$  for SAMs fabricated from  $1^+-CS_2^-$  and  $2^+-CS_2^-$  on gold. All spectra show the expected absorption edge related to the excitation of the C 1s electrons into continuum states and a number of characteristic absorption features. The pre-edge region exhibits peaks near 285.5 eV, related to C 1s  $\rightarrow \pi^*(C=C)$  transitions of the aromatic rings. This resonance is significantly stronger in the case of  $1^+-CS_2^-$ , which is expected in view of the additional phenyl rings in **1**. In  $2^+-CS_2^-$  this peak is only related to the imidazole unit. All spectra exhibit Rydberg/C-H ( $R^*$ ) resonances near 288.1 eV related to the alkyl chains and broad  $\sigma^*$  resonances related to C-C bonds at higher photon energies. The spectra show no signs of chemical impurities such as C=O. The above assignments were made in accordance with ref. 9c,29–33.

The spectra for  $1^+-CS_2^-$  show a pronounced linear dichroism for the  $\pi^*$  resonances, which is highlighted by the  $70^\circ$ – $20^\circ$  difference spectrum. This is a signature of a certain degree of orientational order and molecular alignment in the SAM. The negative polarity of the observed difference peak implies a strongly tilted orientation of the phenyl ring planes in **1** with respect to the surface. Note that for  $1^+-CS_2^-$  the aromatic  $\pi^*$  resonance is representative of both the phenyl rings and the imidazole moieties. The observed dichroism thus represents an average over the different orientations. For  $2^+-CS_2^-$  we observe a weaker difference peak with positive polarity for the  $\pi^*$  imidazole resonance. This indicates an upright, but tilted orientation of the imidazole unit with respect to the surface.

A quantitative analysis of the C K-edge NEXAFS spectra was performed to determine the average molecular tilt angles. The orientation of aromatic units with respect to the surface normal were determined using the  $\pi^*$  transitions. The intensities of these resonances as a function of the X-ray incidence angle  $\Theta$  are evaluated using published procedures for a vector-type orbital.<sup>29</sup> This analysis yields an average tilt angle for the aromatic ring planes versus the surface normal of  $53^\circ \pm 5^\circ$  for  $1^+-CS_2^-$ . This value represents an average over the phenyl and imidazole orientation and the actual tilt angle of the phenyl rings is most likely higher. For the SAMs fabricated from  $2^+-CS_2^-$  we found an

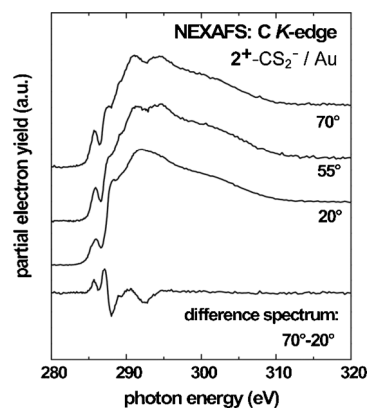


**Fig. 8** C K-edge NEXAFS spectra of SAMs prepared from  $2^+-CS_2^-$  acquired at X-ray incidence angles of  $70^\circ$ ,  $55^\circ$ , and  $20^\circ$ . The bottom curve represents the difference between the  $70^\circ$  and  $20^\circ$  spectra.

average tilt angle  $\Theta$  of  $28^\circ \pm 5^\circ$  for the imidazole unit. The imidazole tilt angle found for this SAM is slightly higher than the corresponding tilt angles found for related aromatic SAMs on gold, such as, for example, SAMs based on biphenyl ( $\Theta \approx 23^\circ$ ), *para*-terphenyl ( $\Theta \approx 20^\circ$ ) or anthracene ( $\Theta \approx 23^\circ$ ) backbones,<sup>34</sup> but it is close to orientations observed for biphenyl tellurolate on gold ( $\Theta \approx 28^\circ$ ).<sup>35</sup> The molecular alignment is superior to SAMs with short aromatic backbones comparable with  $2^+-CS_2^-$ , for example benzene thiol on gold, which have been shown to form mostly disordered layers.<sup>34</sup>

## Conclusion

Our results demonstrate that zwitterionic dithiocarboxylates, which are easily accessible from readily available *N*-heterocyclic carbenes in a single-step reaction with  $CS_2$ , chemisorb intact on solid gold substrates, giving rise to almost contamination-free self-assembled monolayers, which, in view of the absence of extended tailgroups, exhibit a remarkable degree of orientational order. This hitherto neglected adsorbate system has therefore great potential for complementing that of the standard gold-thiolate-based SAMs.<sup>36</sup>

## Experimental

### General considerations

All preparations involving air-sensitive compounds were carried out under an atmosphere of dry nitrogen by using standard Schlenk techniques or in a conventional argon-filled glove box. Solvents and reagents were appropriately dried and purified by conventional methods and stored under inert gas atmosphere. The *N*-heterocyclic carbenes **1**<sup>11b</sup> and **2**<sup>11a</sup> and the azolium salts [3H]Cl<sup>12</sup> and [4H]Br<sup>13</sup> were prepared by slight variation of published procedures. Elemental analyses were carried out by the microanalytical laboratory of the Institute of Thermal Energy Management at the University of Kassel. NMR spectra were recorded with the following Varian spectrometers: VNMRs-500 (500 MHz) and Varian 400-MR (400 MHz). Chemical shifts ( $\delta$ ) are given in ppm and are referenced to the signals due to the

residual protio impurities of the solvents used relative to tetramethylsilane for  $^1\text{H}$  and to the respective solvent signal for  $^{13}\text{C}$ . IR spectra were obtained with a Bruker Alpha-T FT-IR spectrometer (KBr pellets). Raman spectra were obtained at a temperature of 10 K with a Bruker IFS 66/CS FT-NIR spectrometer equipped with a FRA 106 FT-Raman module. An Adlas Nd:YAG laser (350 mW, wavelength 1064 nm) was used as a light source. Optical spectra were obtained with a Perkin Elmer Lambda 40 UV/Vis spectrometer. Mass spectra were obtained with a Bruker Esquire 3000 spectrometer (ESI) and a quadrupole ion-trap spectrometer (ESI and APCI) Finnigan LCQ<sup>DECA</sup> (ThermoQuest, San José, USA).

### Preparative work

**1,3-Bis(2,6-diisopropylphenyl)imidazolium-2-dithiocarboxylate** ( $1^+-\text{CS}_2^-$ ). Carbon disulfide (0.30 mL, 0.38 g, 5.0 mmol) was added to a solution of **1** (1.75 g, 4.5 mmol) in THF (30 mL). The solution was stirred for 15 min. Volatile components were removed *in vacuo*, affording the product as a red microcrystalline solid, which turned out to be analytically pure. Yield 2.06 g (98%). Spectroscopic data were essentially identical to those reported by Delaude *et al.*<sup>4</sup>

**1,3-Diisopropylimidazolium-2-dithiocarboxylate** ( $2^+-\text{CS}_2^-$ ). Carbon disulfide (0.36 mL, 0.46 g, 6.0 mmol) was added to a solution of **2** (614 mg, 4.0 mmol) in THF (25 mL). The solution was stirred for 15 min. Volatile components were removed *in vacuo*. The crude product was purified by column chromatography (silica gel, dichloromethane–ethyl acetate 5 : 1), affording a red microcrystalline solid. Yield 404 mg (76%), mp 232–234 °C.  $^1\text{H}$  NMR:  $\delta$  1.51 (d,  $J = 6.7$  Hz, 12H,  $\text{CH}(\text{CH}_3)_2$ ), 4.96 (sept,  $J = 6.7$  Hz, 2H,  $\text{CH}(\text{CH}_3)_2$ ), 6.99 (s, 2H, = CHN).  $^{13}\text{C}$  NMR:  $\delta$  22.7 50.3, 114.5, 149.0, 225.7. IR (KBr):  $\nu$  3094 (s), 2976 (s), 2931 (m), 2874 (w), 1565 (m), 1479 (s), 1463 (s), 1368 (m), 1211 (s), 1166 (m), 1071 (m), 1047 (s), 753 (w), 716 (s). UV-vis:  $\lambda(\epsilon)$  230 (9500), 266 (7100), 359 (13700), 433 (150), 526 (100). HRMS/ESI(+):  $m/z$  229.0826  $[\text{M}+\text{H}]^+$ , 229.0828 calc. for  $[\text{C}_{10}\text{H}_{16}\text{N}_2\text{S}_2\text{H}]^+$ . Calc. for  $\text{C}_{10}\text{H}_{16}\text{N}_2\text{S}_2$  (228.5): C, 52.56; H, 7.06; N, 12.32. Found: C, 52.18; H, 7.10; N, 12.12%.

**1,3-Dibenzylimidazolium-2-dithiocarboxylate** ( $3^+-\text{CS}_2^-$ ). **[3H]** Cl (650 mg, 2.3 mmol) was stirred for 20 min with 4 Å molecular sieves (*ca.* 2 g) in acetonitrile (25 mL). Potassium-*tert*-butoxide (300 mg, 2.7 mmol) was added and the solution stirred for a further 15 min. Carbon disulfide (0.45 mL, 0.57 g, 7.5 mmol) was added and the solution stirred for a further 15 min. Volatile components were removed *in vacuo*. The crude product was purified by column chromatography (silica gel, dichloromethane–ethyl acetate 5 : 1), affording a dark red microcrystalline solid. Yield 230 mg (31%), mp 178–179 °C (dec.).  $^1\text{H}$  NMR ( $\text{CDCl}_3$ ):  $\delta$  5.29 (s, 4H,  $\text{CH}_2$ ) 6.58 (s, 2H, = CHN), 7.40 (m, 10H, Ph).  $^{13}\text{C}$  NMR ( $\text{CDCl}_3$ ):  $\delta$  51.7, 117.5, 129.2, 129.25, 129.3, 132.8, 150.3, 223.9. IR (KBr):  $\nu$  3162 (w), 3138 (w), 1567 (m), 1496 (s), 1452 (s), 1442 (s), 1360 (m), 1247 (s), 1164 (m), 1056 (s), 966 (w), 749 (m), 730 (m), 711 (s), 691 (m). UV-vis:  $\lambda(\epsilon)$  238 (9000), 256 (10000), 360 (13800), 444 (250), 531 (150). HRMS/ESI(+):  $m/z$  347.0652  $[\text{M} + \text{Na}]^+$ , 347.0647 calc.

for  $[\text{C}_{18}\text{H}_{16}\text{N}_2\text{S}_2\text{Na}]^+$ . Calc. for  $\text{C}_{18}\text{H}_{16}\text{N}_2\text{S}_2$  (324.6): C, 66.60; H, 4.94; N, 8.63. Found: C, 66.39; H, 4.94; N, 8.63%.

**1,3-Diethylbenzimidazolium-2-dithiocarboxylate** ( $4^+-\text{CS}_2^-$ ). Potassium-*tert*-butoxide (146 mg, 1.3 mmol) was added to a solution of **[4H]Br** (281 mg, 1.1 mmol) in THF (25 mL) affording a yellow precipitate. Subsequently, carbon disulfide (120  $\mu\text{L}$ , 152 mg, 2.0 mmol) was added and the mixture stirred for 15 min. Volatile components were removed *in vacuo*. The crude product was purified by column chromatography (silica gel, dichloromethane), affording a dark red microcrystalline solid. Yield 121 mg (44%), mp 211–212 °C (dec.).  $^1\text{H}$  NMR ( $\text{CDCl}_3$ ):  $\delta$  1.59 (t,  $J = 7.3$  Hz, 6H,  $\text{CH}_3$ ), 4.43 (q,  $J = 7.3$  Hz, 4H,  $\text{CH}_2$ ), 7.56 (m, 4H, CH).  $^{13}\text{C}$  NMR ( $\text{CDCl}_3$ ):  $\delta$  14.3, 40.95, 112.4 (2C, 5,8-CH), 126.05 (2C, 6,7-CH), 129.90 (2C, 4,9-C), 152.59 (1C, NCN), 224.01 (1C,  $\text{CS}_2$ ). IR (KBr):  $\nu$  2960 (w), 1501 (s), 1467 (s), 1435 (s), 1380 (m), 1359 (m), 1340 (m), 1138 (w), 1095 (m), 1056 (s), 1034 (m), 1021 (m), 924 (m), 807 (m), 745 (s). UV-vis:  $\lambda(\epsilon)$  229 (12800), 273 (8150), 309 (10850), 362 (10600), 438 (150), 528 (150). HRMS/ESI(+):  $m/z$  273.0497  $[\text{M} + \text{Na}]^+$ , 273.0491 calc. for  $[\text{C}_{12}\text{H}_{14}\text{N}_2\text{S}_2\text{Na}]^+$ . Calc. for  $\text{C}_{12}\text{H}_{14}\text{N}_2\text{S}_2$  (250.5): C, 57.53; H, 5.63; N, 11.27. Found: C, 57.27; H, 5.87; N, 10.69%.

### X-Ray crystal structure determinations

For each data collection a single-crystal was mounted on a glass fibre and all geometric and intensity data were taken from this sample. Data collection using Mo- $K\alpha$  radiation ( $\lambda = 0.71073$  Å) was made on a Stoe IPDS2 diffractometer equipped with a 2-circle goniometer and an area detector. Absorption correction was done by integration using X-red.<sup>37</sup> The data sets were corrected for Lorentz and polarisation effects. The structures were solved by direct methods (SHELXS97) and refined using alternating cycles of least squares refinements against  $F^2$  (SHELXL97).<sup>38</sup> All non H atoms were found in difference Fourier maps and were refined with anisotropic displacement parameters. H atoms were placed in constrained positions according to the riding model with the 1.2 fold isotropic displacement parameters. Crystallographic details are collected in Table 4. Graphical representations were made using ORTEP-3 win.<sup>39</sup>

### Optical second harmonic generation (SHG)

Gold substrates were prepared at the Institute of Nanostructure Technology and Analytics, Kassel University, Germany (200 nm gold with a 15 nm titanium interlayer for adhesion promotion evaporated on an Si(100) wafer). For the SHG measurements the gold substrates were cut to pieces of  $1 \times 1$  cm<sup>2</sup> each and placed in a homemade cuvette, whose quartz glass window was sealed with a Chemraz O-ring. The cuvette was filled with pure dichloromethane at the beginning of the experiments and the pure solvent was subsequently replaced by the solution of the adsorbate species. The adsorption process was measured *in situ* and in real time by SHG by using a ns-pulsed Nd:YAG laser (GCR-170, Spectra Physics) at a repetition rate of 10 Hz with a fundamental wavelength of 1064 nm. The laser beam was incident on the gold surface under an angle of 45° with a fluence of

**Table 4** Crystal data and structure refinement details

	$2^+ - \text{CS}_2^-$	$3^+ - \text{CS}_2^-$	$4^+ - \text{CS}_2^- \cdot \text{CHCl}_3$
Empirical formula	$\text{C}_{10}\text{H}_{16}\text{N}_2\text{S}_2$	$\text{C}_{18}\text{H}_{16}\text{N}_2\text{S}_2$	$\text{C}_{13}\text{H}_{15}\text{Cl}_3\text{N}_2\text{S}_2$
Molecular weight	228.37	324.45	369.74
Crystal size/mm	$0.60 \times 0.45 \times 0.03$	$0.45 \times 0.34 \times 0.09$	$0.19 \times 0.15 \times 0.02$
$T_{\text{min}}/T_{\text{max}}$	0.85/0.98	0.86/0.97	0.88/0.98
$T/\text{K}$	173(2)	193(2)	218(2)
Crystal system	Tetragonal	Monoclinic	Monoclinic
Space group	$P 4_1 2_1 2$	$P 2_1/c$	$P 2_1/n$
$a/\text{\AA}$	9.2048(4)	11.5106(15)	9.1788(10)
$b/\text{\AA}$	9.2048(4)	18.013(2)	14.2940(13)
$c/\text{\AA}$	28.6900(17)	16.037(2)	13.2075(16)
$\beta$ (°)		91.115(10)	94.883(9)
$V/\text{\AA}^3$	2430.9(2)	3324.5(7)	1726.6(3)
$Z$	8	8	4
$D_c/\text{g cm}^{-3}$	1.248	1.296	1.422
$\mu/\text{mm}^{-1}$	0.404	0.318	0.764
$\theta$ range/°	2.32 to 24.99	1.70 to 25.36	2.10 to 25.00
Refl. measured	5036	21 202	7557
Unique refl.	1230	5974	3028
$R_{\text{int}}$	0.0707	0.1497	0.0337
Refl. observed	1148	3083	1980
$R_1, wR_2$ ( $I > 2\sigma(I)$ )	0.0338, 0.0853	0.0812, 0.2047	0.0717, 0.1864
$R_1, wR_2$ (all data)	0.0360, 0.0862	0.1338, 0.2333	0.1038, 0.2048
$\Delta\rho_{\text{min}}/\text{max}/\text{e \AA}^{-3}$	-0.209/0.245	-0.530/0.369	-0.792/0.894

20 mJ cm<sup>-2</sup>. After generation of the second harmonic light, light of the fundamental wavelength was filtered out by using several colour glasses (BG39, Schott) and a monochromator. Finally, the second harmonic signal was detected by a photomultiplier tube and processed with a boxcar for storage on a PC. A fraction of the fundamental laser light was benched off by a dielectric beam splitter. This light was aligned onto a y-cut quartz plate in order to generate a reference SHG signal. It was detected comparable to the signal of the sample and acted to normalise the SHG signal from the sample. Thus, intensity fluctuations of the laser light were minimised. Details of the experimental setup for the investigation of the adsorption and monolayer formation have been published elsewhere.<sup>17</sup>

### X-Ray photoelectron spectroscopy

All XP spectra were collected on a Kratos AXIS Ultra DLD instrument (Kratos, Manchester, England) equipped with a monochromatic Al K $\alpha$  X-ray source (photon energy = 1486.6 eV). The photoelectron take-off angle was normal to the substrate while the photoelectron binding energy scale was calibrated to the Au 4f<sub>7/2</sub> emission (84.0 eV) of the underlying gold substrate. The reported XPS compositions are an average from three spots per sample and calculated from peak areas taken from both a survey scan (0 to 1100 eV for C 1s and Au 4f) and selected region scans (524–544 eV for O 1s; 390–410 eV for N 1s; 155–173 eV for S 2p) acquired at an analyser pass energy of 80 eV. Molecular environments of the samples were characterised by high-resolution (analyser pass energy = 20 eV) spectra from the S 2p, N 1s, and C 1s regions. For all peak quantifications a linear background was subtracted. Peak areas were normalised by the manufacturer-supplied sensitivity factors and surface concentrations were calculated using Casa XPS software.

### Near-edge X-ray absorption fine structure spectroscopy

NEXAFS spectra were recorded at the National Synchrotron Light Source (NSLS) U7A beamline at Brookhaven National Laboratory, using an elliptically polarised beam with ~85% p-polarisation. This beam line uses a monochromator and 600 l mm<sup>-1</sup> grating that provides a full-width at half-maximum (FWHM) resolution of ~0.15 eV at the carbon K-edge (285 eV). The monochromator energy scale was calibrated using the 285.35 eV C 1s  $\rightarrow \pi^*$  transition on a graphite transmission grid placed in the path of the X-rays. C K-edge spectra were normalised by the spectrum of a clean gold surface prepared by evaporation of gold *in vacuo*. Both reference and signal were divided by the NEXAFS signal of an upstream gold-coated reference mesh to account for beam intensity variations.<sup>29</sup> Partial electron yield was monitored with a channeltron detector with the bias voltage maintained at -150 V for C K-edge. The samples were mounted to allow rotation about the vertical axis to change the angle between the sample surface and the incident X-ray beam. The NEXAFS angle is defined as the angle between the incident X-ray beam and the sample surface.

### Acknowledgements

This work was funded in part by NESAC-BIO (NIH grant EB-002027). T. W. and J. E. B. thank David G. Castner for support and Daniel Fischer and Chernoy Jaye (NIST) for providing them with the experimental equipment for NEXAFS spectroscopy and their help at the synchrotron. NEXAFS studies were performed at the NSLS, Brookhaven National Laboratory, which is supported by the U. S. Department of Energy, Division of Materials Science and Division of Chemical Sciences. H. M. thanks Ms U. Cornelissen for recording the Raman spectra.

## References

- 1 For reviews, see: (a) L. Delaude, *Eur. J. Inorg. Chem.*, 2009, 1681–1699; (b) W. Kirmse, *Eur. J. Org. Chem.*, 2005, 237–260; (c) J. Nakayama, *J. Synth. Org. Chem. Jpn.*, 2002, **60**, 106–114; seminal paper: (d) N. Kuhn, H. Bohnen and G. Henkel, *Z. Naturforsch. B: Chem. Sci.*, 1994, **49**, 1473–1480.
- 2 (a) W. Schössler and M. Regitz, *Chem. Ber.*, 1974, **107**, 1931–1948; (b) H. E. Winberg and D. D. Coffman, *J. Am. Chem. Soc.*, 1965, **87**, 2776–2777.
- 3 For a review, see: W. D. Ollis, S. P. Stanforth and C. A. Ramsden, *Tetrahedron*, 1985, **41**, 2239–2329.
- 4 L. Delaude, A. Demonceau and J. Wouters, *Eur. J. Inorg. Chem.*, 2009, 1882–1891.
- 5 See, for example: O. Sereda, A. Blanrue and R. Wilhelm, *Chem. Commun.*, 2009, 1040–1042.
- 6 (a) L. L. Borer, J. V. Kong, P. A. Keihl and D. M. Forkey, *Inorg. Chim. Acta*, 1987, **129**, 223–226; (b) L. L. Borer, J. Kong and E. Sinn, *Inorg. Chim. Acta*, 1986, **122**, 145–148.
- 7 (a) S. Naeem, A. L. Thompson, A. J. P. White, L. Delaude and J. D. E. T. Wilton-Ely, *Dalton Trans.*, 2011, **40**, 3737–3747; (b) S. Naeem, A. L. Thompson, L. Delaude and J. D. E. T. Wilton-Ely, *Chem.–Eur. J.*, 2010, **16**, 10971–10974; (c) S. Naeem, L. Delaude, A. J. P. White and J. D. E. T. Wilton-Ely, *Inorg. Chem.*, 2010, **49**, 1784–1793; (d) T. Sugaya, T. Fujihara, A. Nagasawa and K. Unoura, *Inorg. Chim. Acta*, 2009, **362**, 4813–4822; (e) Q. Willem, F. Nicks, X. Sauvage, L. Delaude and A. Demonceau, *J. Organomet. Chem.*, 2009, **694**, 4049–4055; (f) L. Delaude, X. A. Demonceau and J. Wouters, *Organometallics*, 2009, **28**, 4058–4064; (g) T. Fujihara, T. Sugaya, A. Nagasawa and J. Nakayama, *Acta Crystallogr., Sect. E: Struct. Rep. Online*, 2004, **60**, m282–m284.
- 8 (a) U. Siemeling, S. Rittinghaus, T. Weidner, J. Brison and D. Castner, *Appl. Surf. Sci.*, 2010, **256**, 1832–1836; (b) U. Siemeling, C. Bruhn, F. Brethauer, M. Borg, F. Träger, F. Vogel, W. Azzam, M. Badin, T. Strunskus and C. Wöll, *Dalton Trans.*, 2009, 8593–8604; (c) T. Weidner, F. Brethauer, N. Ballav, H. Motschmann, H. Orendi, C. Bruhn, U. Siemeling and M. Zharnikov, *Langmuir*, 2008, **24**, 11691–11700; (d) T. Weidner, N. Ballav, M. Zharnikov, A. Priebe, N. J. Long, J. Maurer, R. Winter, A. Rothenberger, D. Fenske, D. Rother, C. Bruhn, H. Fink and U. Siemeling, *Chem.–Eur. J.*, 2008, **14**, 4346–4360; (e) U. Siemeling, D. Rother, C. Bruhn, H. Fink, T. Weidner, F. Träger, A. Rothenberger, D. Fenske, A. Priebe, J. Maurer and R. Winter, *J. Am. Chem. Soc.*, 2005, **127**, 1102–1103.
- 9 (a) U. Siemeling, C. Schirmacher, U. Glebe, C. Bruhn, J. E. Baio, L. Árnadóttir, D. G. Castner and T. Weidner, *Inorg. Chim. Acta*, 2011, **374**, 302–312; (b) T. Weidner, J. E. Baio, J. Seibel and U. Siemeling, *Dalton Trans.*, 2012, **41**, 1553–1561; (c) T. Weidner, M. Zharnikov, J. Hoßbach, D. G. Castner and U. Siemeling, *J. Phys. Chem. C*, 2010, **114**, 14975–14982; (d) T. Weidner, N. Ballav, U. Siemeling, D. Troegel, T. Walter, R. Tacke and D. G. Castner, *J. Phys. Chem. C*, 2009, **113**, 19609–19617; (e) T. Weidner, A. Krämer, C. Bruhn, M. Zharnikov, A. Shaporenko, U. Siemeling and F. Träger, *Dalton Trans.*, 2006, 2767–2777.
- 10 (a) T.-C. Lee, P.-C. Chen, T.-Y. Lai, W. Tuntiwechapikul, J.-H. Kim and T. R. Lee, *Appl. Surf. Sci.*, 2008, **254**, 7064–7068; (b) K. Cimatu, H. J. Moore, T. R. Lee and S. Baldelli, *J. Phys. Chem. C*, 2007, **111**, 11751–11755; (c) T.-C. Lee, D. J. Hounihan, R. Colorado, Jr., J.-S. Park and T. R. Lee, *J. Phys. Chem. B*, 2004, **108**, 2648–2653; (d) R. Colorado, Jr., R. J. Villazana and T. R. Lee, *Langmuir*, 1998, **14**, 6337–6340.
- 11 (a) T. Schaub and U. Radius, *Chem.–Eur. J.*, 2005, **11**, 5024–5030; (b) B. R. Dible and M. S. Sigman, *J. Am. Chem. Soc.*, 2003, **125**, 872–873; (c) W. A. Herrmann, C. Köcher, L. J. Gooßen and G. R. J. Artus, *Chem.–Eur. J.*, 1996, **2**, 1627–1636; (d) A. J. Arduengo, III, H. V. R. Dias, R. L. Harlow and M. Kline, *J. Am. Chem. Soc.*, 1992, **114**, 5530–5534.
- 12 L. Leclercq, M. Simard and A. R. Schmitzer, *J. Mol. Struct.*, 2009, **918**, 101–107.
- 13 J. A. V. Er, A. G. Tennyson, J. W. Kamplain, V. M. Lynch and C. W. Bielawski, *Eur. J. Inorg. Chem.*, 2009, 1729–1738.
- 14 C. Furlani and M. L. Luciani, *Inorg. Chem.*, 1968, **7**, 1586–1592.
- 15 J. Nakayama, T. Kitahara, Y. Sugihara, A. Sakamoto and A. Ishii, *J. Am. Chem. Soc.*, 2000, **122**, 9120–9126.
- 16 (a) R. M. Corn and D. A. Higgins, *Chem. Rev.*, 1994, **94**, 107–125; (b) Y. R. Shen, *Annu. Rev. Phys. Chem.*, 1989, **40**, 327–350.
- 17 (a) O. Dannenberger, M. Buck and M. Grunze, *J. Phys. Chem. B*, 1999, **103**, 2202–2213; (b) M. Buck, F. Eisert, M. Grunze and F. Träger, *Appl. Phys. A*, 1995, **60**, 1–12.
- 18 C. Jung, O. Dannenberger, Y. Xu, M. Buck and M. Grunze, *Langmuir*, 1998, **14**, 1103–1107.
- 19 (a) J. D. Andrade, in *Surface and Interfacial Aspects of Biomedical Polymers*, ed. J. D. Andrade, Plenum Press, New York, 1985, vol. 2, ch. 1; (b) I. Langmuir, *J. Am. Chem. Soc.*, 1918, **40**, 1361–1403.
- 20 K. A. Peterlinz and R. Georgiadis, *Langmuir*, 1996, **12**, 4731–4740.
- 21 J. F. Moulder, W. F. Stickle, P. E. Sobol and K. D. Bomben, *Handbook of X-ray Photoelectron Spectroscopy*, Perkin-Elmer Corp., Eden Prairie, 1992.
- 22 D. G. Castner, K. Hinds and D. W. Grainger, *Langmuir*, 1996, **12**, 5083–5086.
- 23 T. Ishida, N. Choi, W. Mizutani, H. Tokumoto, I. Kojima, H. Azebara, H. Hokari, U. Akiba and M. Fujihira, *Langmuir*, 1999, **15**, 6799–6806.
- 24 P. Morf, F. Raimondi, H.-G. Nothofer, B. Schnyder, A. Yasuda, J. M. Wessels and T. A. Jung, *Langmuir*, 2006, **22**, 658–663.
- 25 For a recent review, see: N. Kano and T. Kawashima, *Top. Curr. Chem.*, 2005, **251**, 141–180.
- 26 (a) A. M. Manotti Lanfredi, F. Ugozzoli, F. Asaro, G. Pellizer, N. Marsich and A. Camus, *Inorg. Chim. Acta*, 1992, **192**, 271–282; (b) H. Otto and H. Werner, *Chem. Ber.*, 1987, **120**, 97–104.
- 27 (a) M. Luz Gallego, A. Guijarro, O. Castillo, T. Parella, R. Mas-Balleste and F. Zanora, *CrystEngComm*, 2010, **12**, 2332–2334; (b) J. A. Schuerman, F. R. Fronczek and J. Selbin, *J. Am. Chem. Soc.*, 1986, **108**, 336–337; (c) B. Chiari, O. Piovesana, T. Tarantelli and P. F. Zanazzi, *Inorg. Chem.*, 1985, **24**, 366–371; (d) O. Piovesana and P. F. Zanazzi, *Angew. Chem., Int. Ed. Engl.*, 1980, **19**, 561–562.
- 28 C. L. A. Lamont and J. Wilkes, *Langmuir*, 1999, **15**, 2037–2042.
- 29 J. Stöhr, *NEXAFS Spectroscopy*, Springer, Berlin, 1992.
- 30 D. A. Outka, J. Stöhr, J. P. Rabe and J. D. Swalen, *J. Chem. Phys.*, 1988, **88**, 4076–4087.
- 31 K. Weiss, P. S. Bagus and C. Wöll, *J. Chem. Phys.*, 1999, **111**, 6834–6845.
- 32 P. Väterlein, R. Fink, E. Umbach and W. Wurth, *J. Chem. Phys.*, 1998, **108**, 3313–3320.
- 33 O. M. Cabarcos, A. Shaporenko, T. Weidner, S. Uppili, L. S. Dake, M. Zharnikov and D. L. Allara, *J. Phys. Chem. C*, 2008, **112**, 10842–10854.
- 34 S. Frey, V. Stadler, K. Heister, W. Eck, M. Zharnikov, M. Grunze, B. Zeysing and A. Terfort, *Langmuir*, 2001, **17**, 2408–2415.
- 35 T. Weidner, A. Shaporenko, J. Müller, M. Holtig, A. Terfort and M. Zharnikov, *J. Phys. Chem. C*, 2007, **111**, 11627–11635.
- 36 See, for example: J. C. Love, L. A. Estroff, J. K. Kriebel, R. G. Nuzzo and G. M. Whitesides, *Chem. Rev.*, 2005, **105**, 1103–1170.
- 37 Stoe & Cie, *X-red ver. 1.31, Program for numerical absorption correction*, Darmstadt, Germany, 2004
- 38 G. M. Sheldrick, *Acta Crystallogr., Sect. A: Found. Crystallogr.*, 2008, **64**, 112–122.
- 39 L. J. Farrugia, *J. Appl. Crystallogr.*, 1999, **32**, 837–838.